Study on atomic layer etching of Si in inductively coupled Ar/Cl$_2$ plasmas driven by tailored bias waveforms

Xiaoqin MA (麻晓琴)**, Saiqian ZHANG** (张赛谦)**, Zhongling DAI** (戴忠玲)[1] **and Younian WANG** (王友年)

School of Physics and Optoelectronic Technology, Dalian University of Technology, Dalian 116024, People's Republic of China

E-mail: 1192287760@qq.com and daizhl@dlut.edu.cn

CrossMark

Abstract
Plasma atomic layer etching is proposed to attain layer-by-layer etching, as it has atomic-scale resolution, and can etch monolayer materials. In the etching process, ion energy and angular distributions (IEADs) bombarding the wafer placed on the substrate play a critical role in trench profile evolution, thus importantly flexibly controlling IEADs in the process. Tailored bias voltage waveform is an advisable method to modulate the IEADs effectively, and then improve the trench profile. In this paper, a multi-scale model, coupling the reaction chamber model, sheath model, and trench model, is used to research the effects of bias waveforms on the atomic layer etching of Si in Ar/Cl$_2$ inductively coupled plasmas. Results show that different discharge parameters, such as pressure and radio-frequency power influence the trench evolution progress with bias waveforms synergistically. Tailored bias waveforms can provide nearly monoenergetic ions, thereby obtaining more anisotropic trench profile.

(Some figures may appear in colour only in the online journal)

1. Introduction

Plasma etching is a requisite technology in microelectronics manufacturing, and can transfer fine patterns from mask to other materials with good uniformity [1], selectivity, anisotropy, aspect ratios, and fidelity. However, the booming development of the semiconductor industry demands smaller critical dimensions of integrated circuit devices, which requires the unprecedented control of trench profile evolution to achieve the stringent requirements. Plasma atomic layer etching (PALE) is proposed as a promising method to achieve these goals, as it can obtain the atomic-scale precision control for microelectronics fabrication. The conventional atomic layer etching includes 2-step-recess and the two recesses result in a fatal shortage, the long time to complete a cycle,

which leads to low productivity in the process. Plasma-enhanced atomic layer etching (PEALE) is an effective way to solve this issue by using a mixture of argon and chlorine as the background gas to eliminate the recesses, which then achieves rapid atomic layer etching and improves etching productivity. The basis of PEALE is forming a passivated layer on the top of the etched substrate materials, which decreases the activation energy required by ion bombardment to remove that layer [2]. In addition, the atomic layer etching typically relies on the ion energy and angular distributions (IEADs) incident on the wafer, so that the high-energy ions can provide high etching rates. Nevertheless, these ions may be detrimental to selectivity and result in energy damage. The properties of the sheath region generated above the wafer principally determine the IEADs.

For the past few years, many numerical and experimental investigations have been implemented to study IEADs and

etching processes. Shin *et al* [3] used a retarding field energy analyzer to measure ion energy distributions (IEDs) on a grounded substrate in a Faraday-shielded argon inductively coupled plasma (ICP), and a Langmuir probe to measure plasma parameters. IEDs and plasma parameters were researched with continuous or pulsed positive dc bias on a boundary electrode, which contacted with the plasma. Petit-Etienne *et al* [1] used a 300 mm AdvantEdge™ ICP etch tool to investigate the simplistic situation of silicon etching in a chlorine plasma. Their results show promise for plasma etching processes requiring control at the atomic level. Numerical investigations can provide insight into the physics mechanism and help in obtaining ideal discharge conditions to optimize the etching processes [4]. Economou [5] applied 'tailored' voltage waveforms to control the IEDs on plasma electrodes. However, this view only discussed electropositive plasma. Denpoh [6] coupled the Monte Carlo model with a polydimensional radio-frequency (RF) sheath model to simulate the IEADs. However, the RF sheath cannot remit the charge accumulation effects on insulating substrates efficiently. Charging effects will alter the distribution of the electric field in the trench, and then influence the IEADs [7]. Liu *et al* [8] employed a voltage compensation method to eliminate the charging effect. In their work, they employed argon as the discharge gas, but did not take the reactive gases into account. Agarwal *et al* [2] used the hybrid plasma equipment model (HPEM) to demonstrate the feasibility of using conventional plasma equipment for PALE processes. Hoekstra *et al* [9] described a 2D plasma chemistry Monte Carlo simulation (PCMCS), which was used to track the trajectory of ions and neutrals as a function of phase during the RF cycle, for IEDs onto the wafer in ICP reactors for etching. However, they had not considered influential factors, such as charging and local surface coverage. Agarwal *et al* [10] discussed the effects of different pulse parameters on the pulsed plasma characteristics, IEADs, and trench profile evolution of Si etching in Ar/Cl$_2$ plasma. They found that the bulk plasma properties are strongly impacted by the source power deposition, while the energy and angular distributions of ions incident onto the wafer are sensitive to the pulse-bias shape and the overlap of the source and bias powers. Ranjan *et al* [11] used chlorine and argon plasma in a radial line slot antenna plasma source as a platform to illustrate how cycle time, ion energy, and radical-to-ion ratio can be manipulated to manage the deviation from ideality when cycle times are shortened or purges are incomplete. Zhang *et al* [12] coupled the global model, sheath model, and trench model to study the etching of Si in chlorine plasmas. Nevertheless, the densities and fluxes of ions and neutrals obtained from the global model are not precise enough. Tinck *et al* [13] used the HPEM to study the effects of different parameters on the plasma properties and on the fluxes and energies of ions and neutrals impacting on the substrate, compared with the etch rates measured by the experimental method to investigate the etch process for Si etching based on Ar/Cl$_2$ ICPs.

In this paper, a multi-scale model [12], which included a reaction chamber, sheath model, and trench model, is used to study the effects of different parameters, for instance, gas
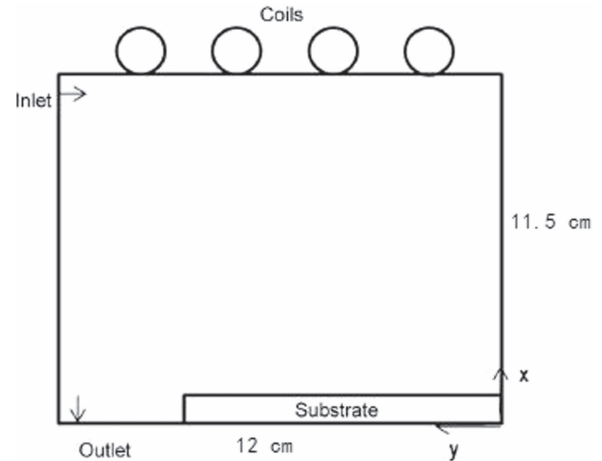

Figure 1. Schematic diagram of the ICP reactor chamber model.

pressure, source power, and bias voltage waveforms, on the trench profile evolution. The brief descriptions of models are presented in section 2. The results and discussions are presented in section 3. The conclusions are presented in section 4.

2. Model descriptions

To study the atomic layer etching in the ICP, the commercial solver CFD-ACE+ [14] is used to built an ICP reactor model, to simulate the discharges in the reactor and give the densities and fluxes of ions and neutrals used as boundary conditions in the 1D hybrid sheath model [12, 15]. The sheath model combined the fluid model with the Monte Carlo model, and is used to calculate the IEADs. Then, the 2D trench model uses the fluxes of etchant particles and the IEADs as input parameters to simulate the evolution of the trench feature.

2.1. Reactor model

In this article, the inductively coupled discharge is created by RF current passing through a multi-turn planar coil situated on the top of the reactor chamber, and the RF is 13.56 MHz. The ICP reactor model is shown in figure 1. The radius of the chamber is 12 cm, and the distance between the top of the chamber and substrate is 11.5 cm.

The chemistry, heat, flow, electric, and magnetic modules in CFD-ACE+ are coupled to the plasma module to accommodate features for plasma simulations. In the ICP model, the plasma module solves the electron energy balance equation and uses the quasi-neutrality condition to calculate the electron density and electrostatic field. The fluxes, densities of ions and neutrals are obtained from the species transport equations in the chemistry module [14].

The electron density n_e in CFD-ACE+ is expressed as follows:

$$n_e = \sum q_i n_i \qquad (1)$$

where n_i denotes the ion number densities, q_i is the charge numbers of ions.

The electron density flux is solved from the drift diffusion approximation:

$$\Gamma_e = \mu_e n_e \nabla\varphi - D_e \nabla n_e \qquad (2)$$

where μ_e is the electron mobility, D_e is the diffusion coefficient, and φ is the electrostatic potential.

The electron energy balance equation is used for the electron temperature:

$$\frac{3}{2}\frac{\partial}{\partial t}(n_e T_e) + \nabla\left(\frac{5}{2}T_e\Gamma_e - \chi\nabla T_e\right) = P - n_e\sum_r n_r k_r \varepsilon_r \quad (3)$$

where convective flux and thermal diffusion result in the energy transfer, with the coefficient $\chi = \frac{5}{2}n_e D_e$. The last term on the RHS represents the electron energy loss, which is due to the electron-induced reactions. The power density P stands for the energy absorbed by electrons.

For species transport in plasma, ion drift effect needs to be considered. The mass flux of different species can be expressed as shown below:

$$J_i = -\rho D_i \nabla Y_i + \rho U_{di} Y_i + J_i^c \qquad (4)$$

where Y_i is the species mass fraction, ρ is mass density, D_i is the diffusion coefficient. The first term is due to the concentration gradient, and the second term the drift velocity. The third term is the correction to ensure species flux conservation.

In the low-pressure sheath, the ion momentum equation is expressed as follows:

$$\frac{\partial n_i V_i}{\partial t} + \nabla \cdot n_i V_i V_i = -\frac{1}{m_i}\nabla(k_B n_i T_i) + \frac{q_i e}{m_i}E n_i - \upsilon_{im}n_i V_i$$
$$(5)$$

where the ion collision frequency υ_{im} and ion mobility μ_i is related as $\mu_i = \frac{e}{m_i \upsilon_{im}}$ and the drift velocity is then expressed as:

$$U_{di} = V_i - \sum_j V_j Y_j. \qquad (6)$$

Accurately, mobility of ions is calculated by the Langevin formula:

$$\mu_{ij} = \frac{13.853 \times 10^{-4}}{\sqrt{\alpha_j m_r}} \qquad (7)$$

where α_j represents the polarizability measured in $\mathring{A}^3$ and m_r represents the reduced mass of ions and neutrals [16].

The temperature of ions and neutrals is obtained from the enthalpy balance equation and assumed to be the same. In gas-phase reactions, we only consider the collisions of electrons with ionic species and neutral particles, because ions cannot be accelerated easily by the electric field, which means that the reactions between heavy particles can be ignored compared to the electron-impact reactions.

The gas-phase reactions taken into account in this article are shown in table 1.

2.2. Sheath model

There will be a sheath region formed at the contiguous area of the substrate. The properties of the sheath play a critical role in the determination of the ion transport characteristics. Ions get energy when passing through the sheath, which is crucial to the ion fluxes and energy bombarding the substrate, eventually affecting the surface process. For the purpose of controlling the generation of plasmas and ion transportation independently in low-pressure and high-density plasmas, a separate bias applied on the bias electrode can be used.

In this section, a hybrid sheath model [12, 15] coupled with the fluid model and Monte Carlo model, is presented to calculate the IEADs. The fluid model can be used to compute the temporal-spatial variables, such as electric potential and sheath thickness, etc. Then, the Monte Carlo method, in which the collisions between ions and neutrals are taken into account, is applied to get the IEDs and ion angular distributions (IADs). The 1D hybrid sheath model is shown as follows [8]:

Due to the fact that the thermal velocity of ions is much smaller than the directional velocity in the sheath area, the ion thermal motion effects can be ignored. Therefore, ion density $n_i(x, t)$, ion velocity $u_i(x, t)$, and the electric potential $V_i(x, t)$ can be calculated from the cold fluid equations:

$$\frac{\partial u_i}{\partial t} + u_i\frac{\partial u_i}{\partial x} = -\frac{q}{m_i}\frac{\partial V}{\partial x} - \upsilon u_i \qquad (8)$$

$$\frac{\partial n_i}{\partial t} + \frac{\partial(n_i u_i)}{\partial x} = 0 \qquad (9)$$

where m_i represents the ion mass, q represents the ion charges, υ represents the ion-neutral collision frequency.

We consider the electric potential through the Poisson equation:

$$\frac{\partial^2 V_i}{\partial x^2} = -\frac{e}{\varepsilon_0}(n_+ - n_- - n_e) \qquad (10)$$

where ε_0 is vacuum permittivity and n_e represents the electron density, which satisfies the Boltzmann relation:

$$n_e(x, t) = n_0 \exp\left(\frac{eV(x, t)}{k_B T_e}\right) \qquad (11)$$

where n_0 represents the density of bulk plasma, T_e represents the electron temperature, and k_B represents the Boltzmann constant.

Furthermore, the appropriate conditions are necessary to solve the above-mentioned equations. Ions will obtain kinetic energy when passing through the pre-sheath region, and then enter into the sheath region with Bohm velocity. As shown bellow, the modified Bohm critical [11] is

$$u_i(d_s, t) \geqslant \left[\frac{eT_e(1 + \alpha_s)}{M(1 + \alpha_s\gamma)}\right]^{1/2} \qquad (12)$$

where $\alpha_s \equiv n_-/n_e$ represents the ratio of negative ions to electrons, $\gamma = T_e/T_i$ represents the temperature ratio of electrons to ions, d_s is the position of the plasma-sheath boundary represented in figure 2, and is decided by the quasi-neutral state

Table 1. Gas-phase chamber reactions for Ar/Cl₂ plasma.

Reaction[a]	Ap	n	Ea/R	Notes
Electron-impact reactions				
1 $Ar + e \rightarrow Ar^+ + 2e$	0	0	0	[b]
2 $Ar + e \rightarrow Ar^* + e$	0.2E-014	0	11.94	[c]
3 $Ar^* + e \rightarrow Ar^+ + 2e$	3E-013	0.1	5.22	[c]
4 $Ar + e \rightarrow Ar + e$	0	0	0	[b]
5 $Cl_2 + e \rightarrow Cl_2^+ + 2e$	0	0	0	[b]
6 $Cl_2 + e \rightarrow Cl^- + Cl$	0	0	0	[b]
7 $Cl_2 + e \rightarrow 2Cl + e$	0	0	0	[b]
8 $Cl^- + e \rightarrow Cl + 2e$	3.28E-014	0	5.37	[c]
9 $Cl + e \rightarrow Cl^+ + 2e$	3E-014	0.559	13.21	[c]
10 $Cl_2 + e \rightarrow Cl^+ + Cl + 2e$	3.88E-015	0	15.5	[c]
11 $Cl_2 + e \rightarrow Cl^+ + Cl^- + e$	0	0	0	[b]
Ion recombination reactions				
12 $Cl_2^+ + Cl^- \rightarrow Cl + Cl_2$	5E-014	0	0	[c]
13 $Cl^+ + Cl^- \rightarrow 2Cl$	5E-014	0	0	[c]

[a] All the rate coefficients are given from CFD-ACE+.
[b] Rate coefficients in CFD-ACE+ are calculated by the collision cross-section, which are taken from www.eeel.nist.gov/811/refdata.
[c] Rate coefficients are calculated by the Arrhenius method, with the equation … Unit of A is molecules^{-1}cm^3 s^{-1} for bimolecular reaction. n is temperature coefficient in Kelvin, m is pressure coefficient and set zero, and Ea is activation energy in eV [17].
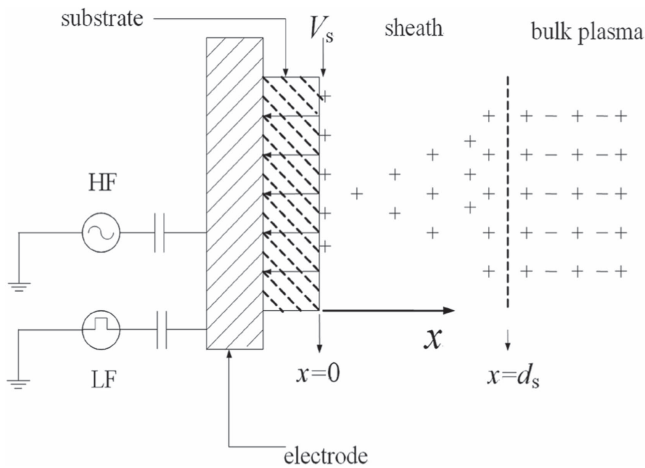
Figure 2. Schematic diagram of the 1D sheath model.

at the sheath edge:

$$n_+(d_s, t) = n_e(d_s, t) + n_-(d_s, t). \quad (13)$$

In addition, we suppose that the potential at the sheath edge is

$$V(0, t) = V_e(t) \quad (14)$$
$$V(d_s, t) = 0 \quad (15)$$

where $V_e(t)$ represents the amplitude of bias voltage, which is applied on the electrode, and $V(d_s, t)$ represents the electric potential at the sheath edge.

We can only get a perspective of the sheath properties from the fluid model. In order to accurately calculate the information of ion energy and ion angle, we must use the Monte Carlo model to take the ion-neutral collisions into

account, and then obtain the IEADs. Since the density of ions is much smaller than that of neutrals, the ion-ion collisions can be ignored, and we can only consider the ion-neutral collisions. Charge exchange (cx) collisions and elastic (el) collisions are the collision progresses we considered in this paper. For Ar$^+$-Ar collisions, the collision cross-sections are given in [18, 19], and on the basis of the size of the chlorine atom compared to the argon atom, Cl$^+$-Cl collision cross-sections are described as follows [12]:

$$\sigma_{cx} = 57.2 \times (1.0 - 0.0577 \ln \varepsilon)^2 \quad (16)$$

$$\sigma_{el} = 48.05 \times (1.0 - 0.0563 \ln \varepsilon)^2 \quad (17)$$

where the cross-section is in 10^{-20} m^2 where ion impact energy is in eV. When molecular ions or neutrals are considered in the two-body collisions, we can assume that the cross-section is proportional to all the atom number of species in the collision to modify the cross-sections [12].

In the Monte Carlo model, we can determine what has occurred according to the mean free path, and the kind of collision according to the different cross-sections. The scattering angle and velocity of ions after collisions would be recorded repeatedly until the ion arrives at the substrate surface. Finally, we can get the IEDs and IADs on the substrate by analyzing all the ion energies and angles statistically.

2.3. Trench model

Etching yield (number of Si atoms removed per incident ion) is an important value as a function of key parameters such as IEDs and IADs bombarding the substrate [20]. The trench model [12] uses the fluxes of reactive species and

IEADs as input parameters to simulate the feature profile evolution. After passing through the sheath region, ions would have got enough kinetic energy to activate the desired reactions. Intricate factors would affect the trench profile synchronously.

For the purpose of simulating the trench evolution numerically, we divide the trench domain into grid cells and use a cellular removal method to study the trench profile evolution [12]. The ion trajectories in the trench will be distorted under the local electric field there, which will lead to a non-ideal feature profile, and as in micro- and nano-meter scale patterns, the trench scale is much smaller than the ion mean free path, and so we can use the Laplace equation instead of the Poisson equation to calculate the local electric field

$$\nabla^2 V = 0. \tag{18}$$

Then, we utilize the motion equation under the electric field to describe the trajectory of ions and neutrals in the trench and record the position they reach at the trench surface

$$\frac{d^2 x}{dt^2} = -\frac{q}{m_i}\frac{dV}{dx} \tag{19}$$

where m_i represents the ion mass, and q represents the charge number for electron and ions.

It is worth noting that the ion scattering will influence trench profile evolution significantly when taking the ion-wall interactions into account. The ions will be concentrated upon both sides of the trench bottom after reflecting from the wall, which would result in micro-trenching. In our article, we consider the simplified situation that when ions impact on the surface they will reflect specularly at grazing angles and the collision between the plasma species and wall is elastic, and there is no energy loss in the progress, so that we can use molecular dynamics to predict ion behavior precisely when and after their incidence on the wall, but this requires vast computational costs. Moreover, low-energetic ions will be reflected at random when they arrive at the surface [21] or attach there. Here, the ion reflection will happen if the off-normal angle incident onto the surface is larger than 30 eV, and the reflection will not be probable when the ion kinetic energy is less than 30 eV, and the ions even incide with large off-normal angles [12]. Table 2 gives the surface reactions for the polysilicon etch mechanism shown in [22] that we considered in this paper.

3. Results and discussions

In this article, we simulate the atomic layer etching of Si in the inductively coupled argon/chlorine plasma driven by tailored bias waveforms. We just display the spatial distributions of the dominated reactive ions, such as Ar^+, Cl^+, and Cl_2^+, in the etching process.

The spatial distributions of Ar^+, Cl^+, and Cl_2^+ in the chamber corresponding to different discharge conditions are shown in figures 3–5. Intuitively, all the ion densities decrease from the center of the reaction chamber to the edges.

Table 2. Surface reactions for the polysilicon etch mechanism.

Reaction[a]	Probability for reaction[b]	Reference
$Si_{(s)} + Cl_{(g)} \rightarrow SiCl_{(s)}$	0.99	[22]
$SiCl_{(s)} + Cl_{(g)} \rightarrow SiCl_{2(s)}$	0.20	[22]
$SiCl_{2(s)} + Cl_{(g)} \rightarrow SiCl_{3(s)}$	0.15	[22]
$SiCl_{3(s)} + Cl_{(g)} \rightarrow SiCl_{4(g)}$	0.0001	[22][c]
$Si_{(s)} + SiCl_{2(g)} \rightarrow Si_{(s)} + SiCl_{2(s)}$	0.8	[22]
$SiCl_{(s)} + SiCl_{2(g)} \rightarrow SiCl_{(s)} + SiCl_{2(s)}$	0.5	[22]
$SiCl_{2(s)} + SiCl_{2(g)} \rightarrow SiCl_{2(s)} + SiCl_{2(s)}$	0.3	[22]
$SiCl_{3(s)} + SiCl_{2(g)} \rightarrow SiCl_{3(s)} + SiCl_{2(s)}$	0.1	[22]
$SiCl_{2(s)} + Ar^+ \rightarrow SiCl_{2(g)} + Ar_{(g)}$	$0.16\frac{(\varepsilon - \varepsilon_0)^{1/2}}{\varepsilon_0^{1/2}}$	[23][d]
$SiCl_{3(s)} + Ar^+ \rightarrow SiCl_{3(g)} + Ar_{(g)}$	$0.16\frac{(\varepsilon - \varepsilon_0)^{1/2}}{\varepsilon_0^{1/2}}$	[23][d]
$SiCl_{(s)} + Cl^+ \rightarrow SiCl_{2(g)}$	$0.13\frac{(\varepsilon - \varepsilon_0)^{1/2}}{\varepsilon_0^{1/2}}$	[23][d]
$SiCl_{2(s)} + Si_{(s)} + Cl^+ \rightarrow SiCl_{2(g)} + SiCl_{(s)}$	$0.16\frac{(\varepsilon - \varepsilon_0)^{1/2}}{\varepsilon_0^{1/2}}$	[23][d]
$SiCl_{3(s)} + Cl^+ \rightarrow SiCl_{4(g)}$	$0.19\frac{(\varepsilon - \varepsilon_0)^{1/2}}{\varepsilon_0^{1/2}}$	[23][d]
$Si_{(s)} + Cl_2^+ \rightarrow SiCl_{2(g)}$	$0.13\frac{(\varepsilon - \varepsilon_0)^{1/2}}{\varepsilon_0^{1/2}}$	[23][d]
$SiCl_{(s)} + Si_{(s)} + Cl_2^+ \rightarrow SiCl_{2(g)} + SiCl_{(s)}$	$0.16\frac{(\varepsilon - \varepsilon_0)^{1/2}}{\varepsilon_0^{1/2}}$	[23][d]
$SiCl_{2(s)} + Si_{(s)} + Cl_2^+ \rightarrow SiCl_{2(g)} + SiCl_{2(s)}$	$0.16\frac{(\varepsilon - \varepsilon_0)^{1/2}}{\varepsilon_0^{1/2}}$	[23][d]
$SiCl_{3(s)} + Si_{(s)} + Cl_2^+ \rightarrow SiCl_{4(g)} + SiCl_{(s)}$	$0.19\frac{(\varepsilon - \varepsilon_0)^{1/2}}{\varepsilon_0^{1/2}}$	[23][d]

[a] Subscript (s) represents a surface species. Subscript (g) represents a gas or plasma species.
[b] ε represents ion energy. $\varepsilon_0 = 10$ eV unless noted otherwise [22].
[c] Thermal etch probability was various for some cases as noted [22].
[d] Reaction mechanism was derived from the cited reference. The precise values for probabilities were modified [22].

Comparing (a) with (c) in figures 3–5 respectively, we can find that all the ion densities become larger as the discharge pressure increases, since the increasing discharge pressure is beneficial to discharging, resulting in a higher ionization rate. Comparing (a) with (b) in figures 3–5 separately, reveals that the ion densities will increase with the source power increasing. The increase in source power will bring about higher average electron temperature, which hence increases the formation of ions by electron-impact reactions.

IEADs on the substrate play a critical role in the control of more precise trench profile evolution that the booming development of microelectronics manufacturing demands. Tailored bias voltage is usually applied on the electrode to modulate the IEADs flexibly and narrow the spread in energy, which then provides near monoenergetic ions [1]. In this article, three tailored bias voltage waveforms are applied on the electrode, as shown in figure 6. The amplitude of RF bias is 30 V, and the amplitude of pulsed bias is 160 V. The RF frequency is $f_{rf} = 30$ MHz, and the pulse frequency is $f_{pulse} = 500$ kHz.

Figure 7 represents the IEDs that arrived at the substrate surface under the different tailored bias voltage waveforms
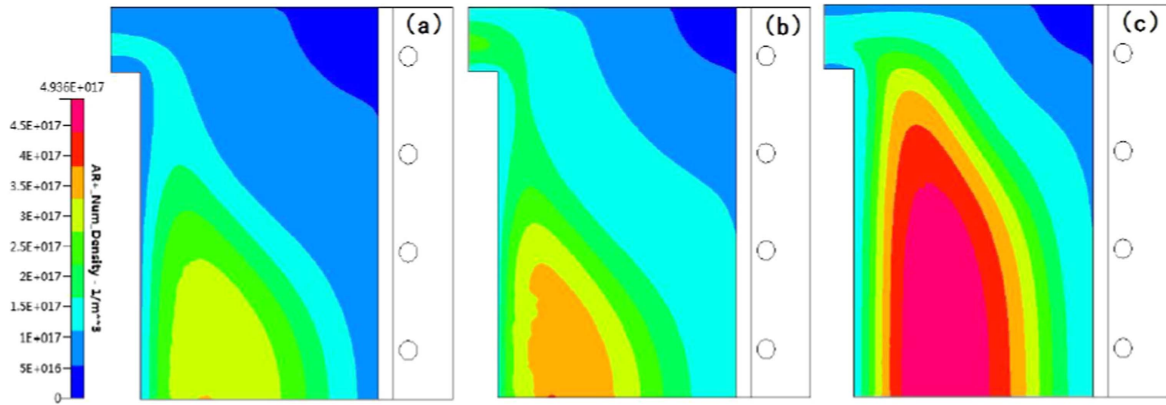
Figure 3. Spatial distributions of Ar$^+$ density in the chamber corresponding to different discharge conditions. Ratio of gas mixture is Ar/Cl$_2$ = 80/20. (a) Pressure = 5 mTorr, power = 300 W, (b) pressure = 5 mTorr, power = 500 W, (c) pressure = 10 mTorr, power = 300 W.
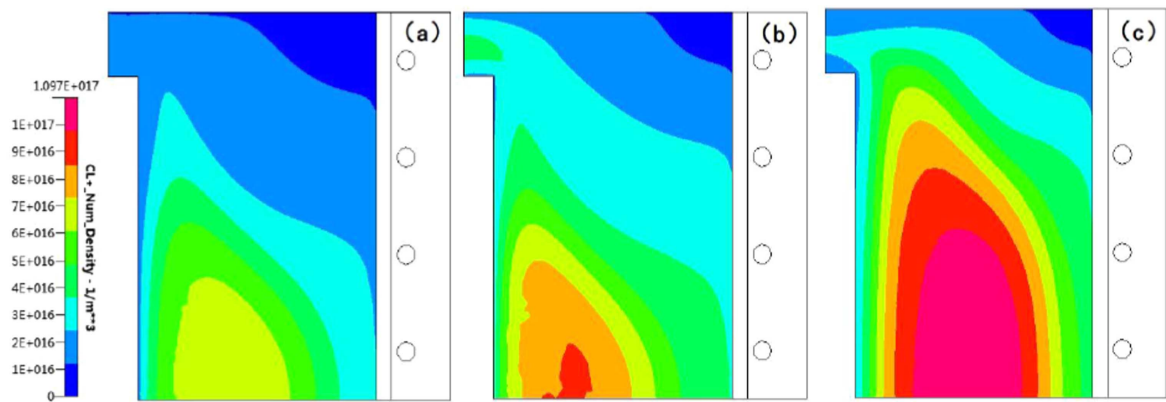
Figure 4. Spatial distributions of Cl$^+$ density in the chamber corresponding to different discharge conditions. Ratio of gas mixture is Ar/Cl$_2$ = 80/20. (a) Pressure = 5 mTorr, power = 300 W, (b) pressure = 5 mTorr, power = 500 W, (c) pressure = 10 mTorr, power = 300 W.
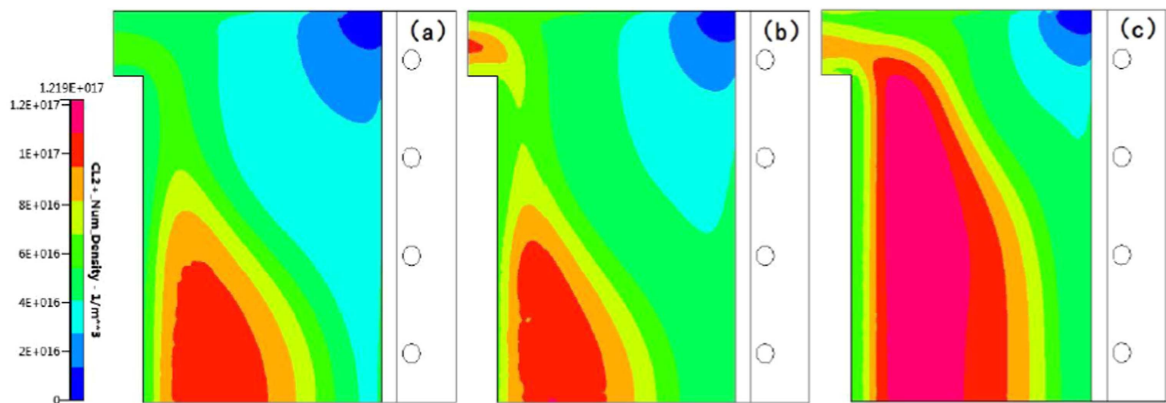
Figure 5. Spatial distributions of Cl$_2{}^+$ density in the chamber corresponding to different discharge conditions. Ratio of gas mixture is Ar/Cl$_2$ = 80/20. (a) Pressure = 5 mTorr, power = 300 W, (b) pressure = 5 mTorr, power = 500 W, (c) pressure = 10 mTorr, power = 300 W.

shown in figure 6. The pressure is 5 mTorr, source power is 300 W, and the ratio of gas mixture is Ar/Cl$_2$ = 80/20. Clearly, the IEDs corresponding to (b) in figure 6 are more homogeneous than those corresponding to (a) and (c). In figure 6(a), all three cycle stages are RF waveforms, which leads to the three bimodal energy distributions shown in
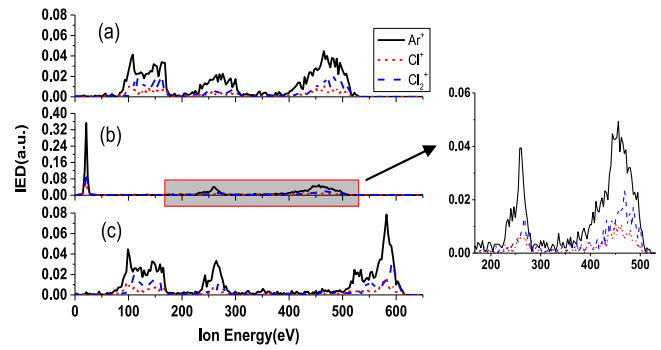
figure 7(a). However, the bimodal character is not obvious. This is because the RF of 30 MHz is so high that ions cannot respond to the fast electric oscillation immediately when they are passing through the sheath region, and the ion energies arriving at the substrate are determined by the average electric field, not the instantaneous electric field. The unimodal
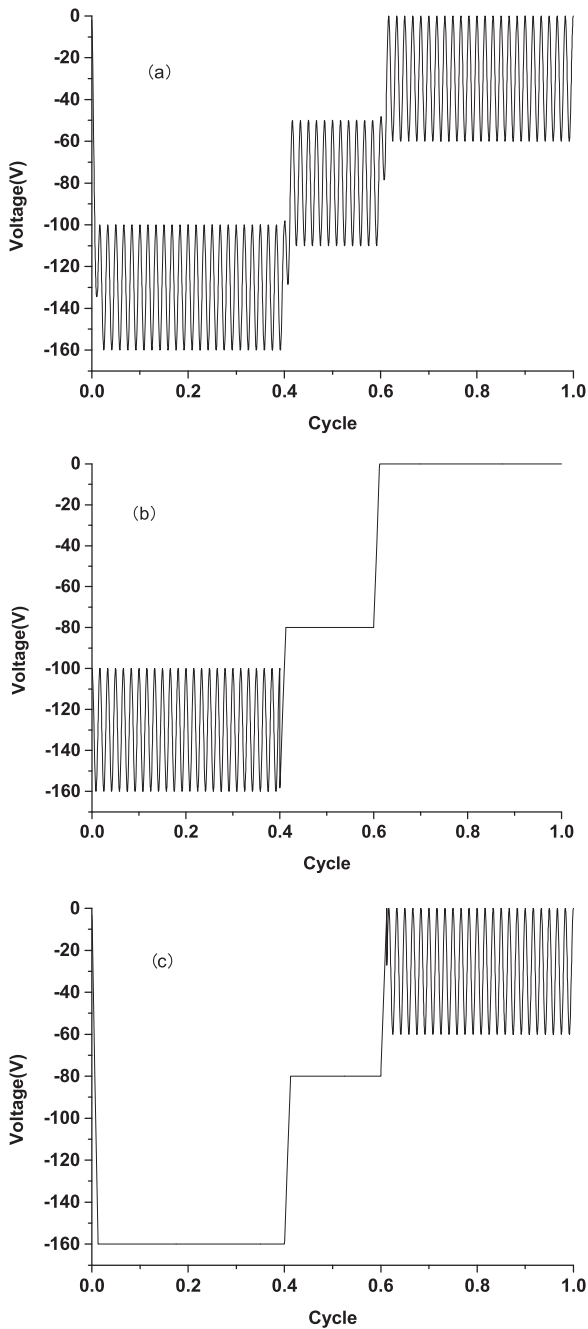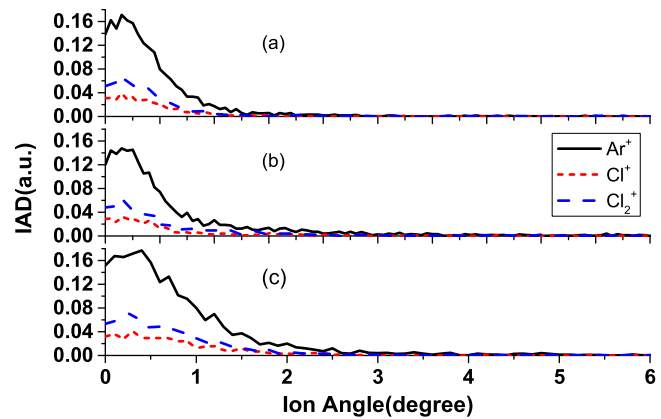
Figure 6. Different tailored bias voltage waveforms applied on the electrode.
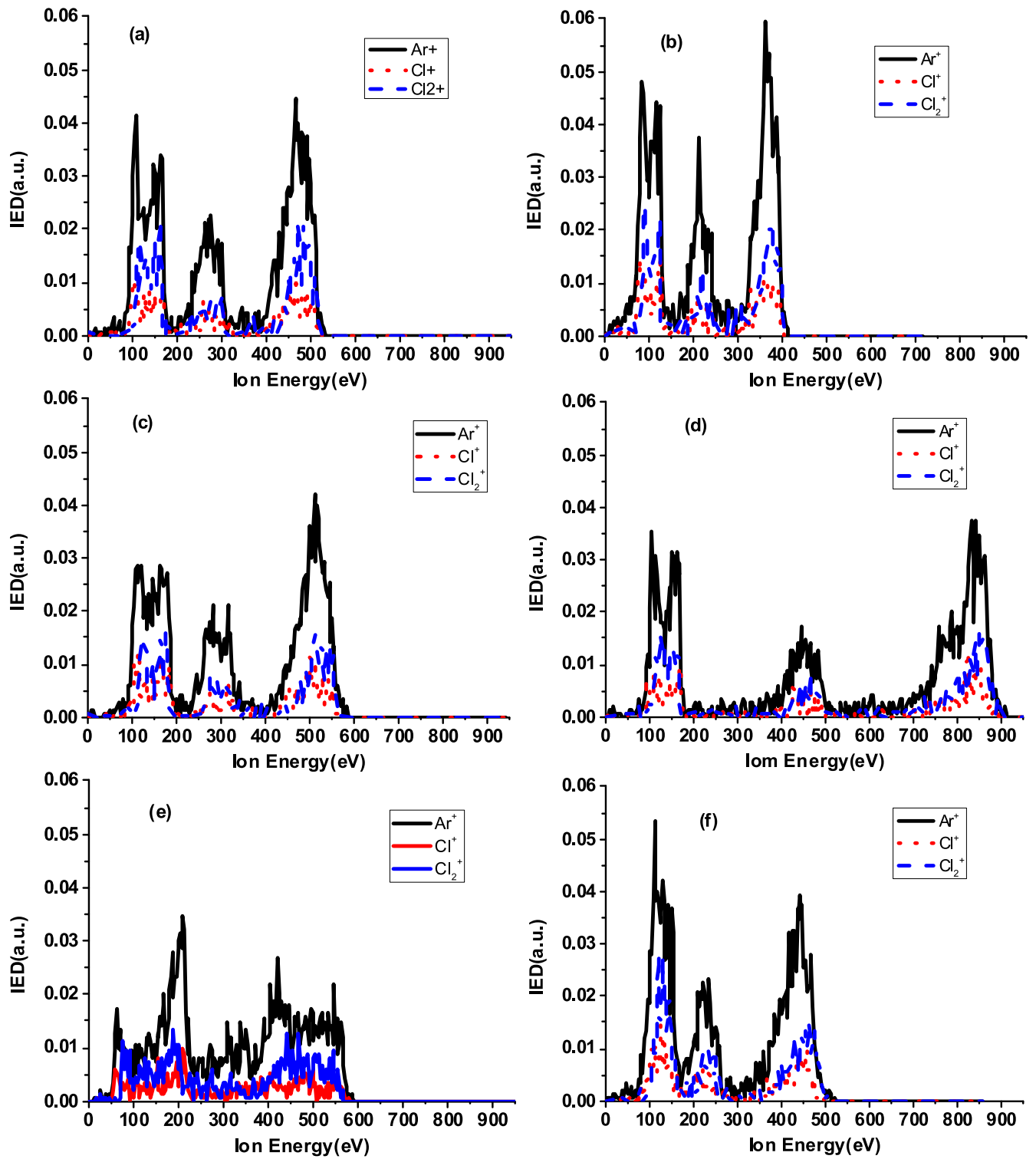

Figure 7. IEDs that arrived at the substrate surface correspond to the bias voltage waveforms shown in figure 6.

Figure 8. IADs that arrived at the substrate surface correspond to the bias voltage waveforms shown in figure 6.

energy distribution in the low-energy region shown in figure 7(b) correspond to the third stage shown in figure 6(b). Similarly, the unimodal energy distributions in the high-energy region shown in figure 7(c) correspond to the first stage shown in figure 6(c).

Figure 8 shows the IADs that arrived at the substrate correspond to the different bias voltage waveforms represented in figure 6. It reveals that more ions incident onto the substrate with more concentrated angles correspond to (c), shown in figure 6, than those that correspond to (a) and (b), which is because the electrode potential drop only influences the perpendicular acceleration to the substrate and the larger

pulse-bias voltage, shown in figure 6(c), results in better directionality of ions moving to the substrate.

We investigate the IEDs and IADs under different exoteric parameters with applying the tailored bias voltage waveform shown in figure 6(a). The ratio of gas mixture is $Ar/Cl_2 = 80/20$. Figure 9 shows the IEDs under different discharge parameters. Figures 9(a) and (b) indicate that when the pressure increases, there will be more ions moving to the low-energy region. This is because the pressure increasing leads to more frequent ion-neutral collisions, and thereby the energetic ions will transfer their energies to neutrals through collision. The IEDs shown in figures 9(a) and (c) reveal that increased source power will result in more ions in the high-energy region. It is not too hard to find that the ion energy distributions extend to the high-energy area as the pulse-bias voltage increases, as shown in figures 9(a) and (d). The high- and low-energy peak correspond to the maximum and minimum of electrode potential, respectively, and the electrode potential will increase with the bias voltage increased, which causes the IEDs to move to the high-energy area. In addition, the electrode potential drop across the sheath region will be larger with the amplitude of bias increases, and ions will obtain more energy when passing through the sheath. From figures 9(a) and (e), we can find that with the RF-bias frequency increases, the IEDs will be more concentrated, and the width between the two peaks reduces rapidly. The large inertia of ions prevents them from responding to the fast
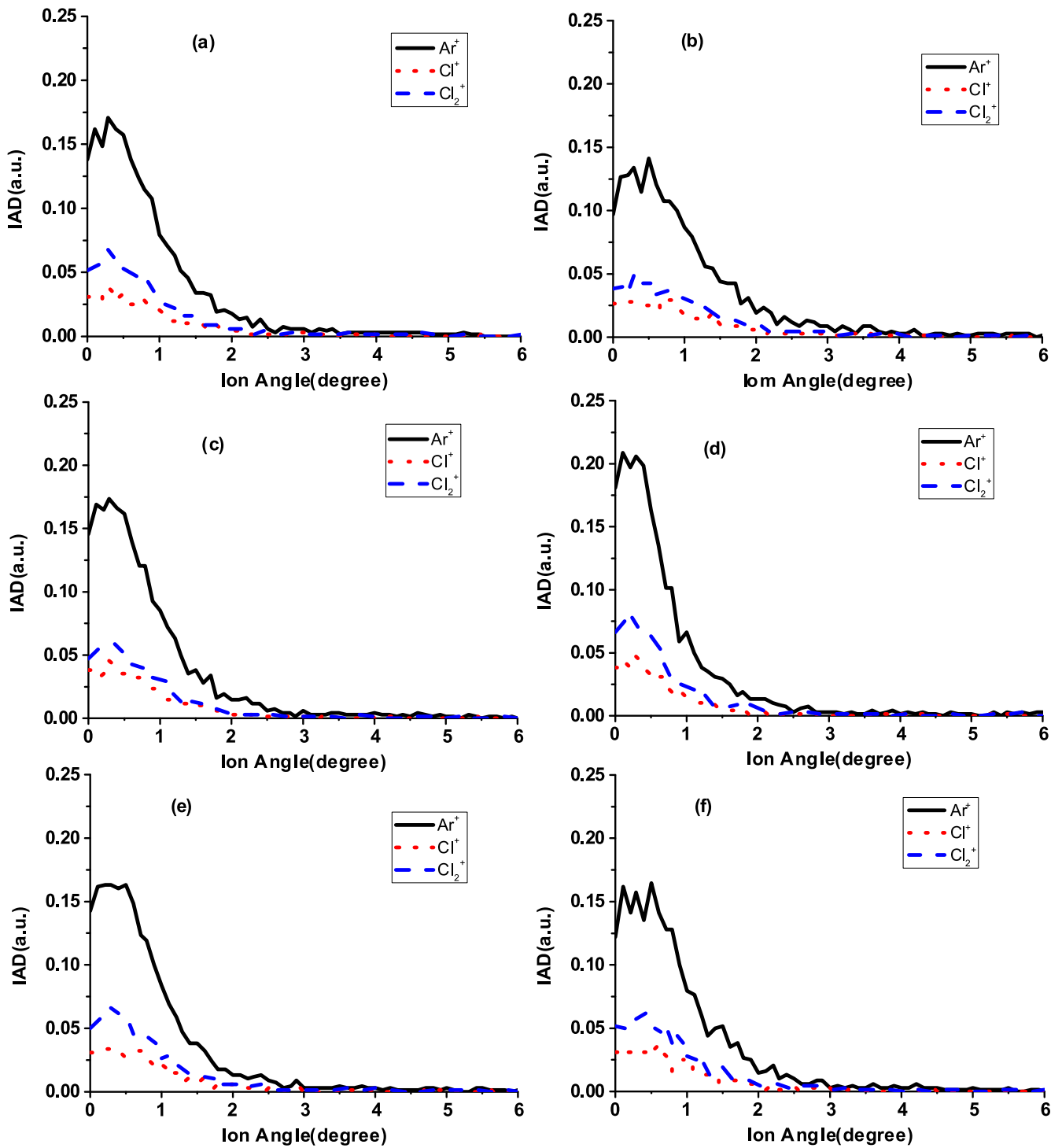
Figure 9. IEDs that arrived at the substrate under different discharge parameters. (a) Pressure = 5 mTorr, power = 300 W, V_{pulse} = 100 V, f_{rf} = 30 MHz, f_{pulse} = 500 kHz. (b) Pressure = 10 mTorr, power = 300 W, V_{pulse} = 100 V, f_{rf} = 30 MHz, f_{pulse} = 500 kHz. (c) Pressure = 5 mTorr, power = 500 W, V_{pulse} = 100 V, f_{rf} = 30 MHz, f_{pulse} = 500 kHz. (d) Pressure = 5 mTorr, power = 300 W, V_{pulse} = 200 V, f_{rf} = 30 MHz, f_{pulse} = 500 kHz. (e) Pressure = 5 mTorr, power = 300 W, V_{pulse} = 100 V, f_{rf} = 13.56 MHz, f_{pulse} = 500 kHz. (f) Pressure = 5 mTorr, power = 300 W, V_{pulse} = 100 V, f_{rf} = 30 MHz, f_{pulse} = 300 kHz.

electric oscillation instantaneously to get sufficient energy from the electric field while transporting across the sheath. Nevertheless, the IEDs displayed in figures 9(a) and (f) show that the effects of pulse-bias frequency increasing on the IEDs are not as conspicuous as those of RF-bias frequency increasing. The position of low-energy peaks is almost settled with the pulse-bias frequency increased, and the high-energy peaks extend to the high-energy region slightly.

Figure 10. IADs that arrived at the substrate under different discharge parameters. (a) Pressure = 5 mTorr, power = 300 W, V_{pulse} = 100 V, f_{rf} = 30 MHz, f_{pulse} = 500 kHz. (b) Pressure = 10 mTorr, power = 300 W, V_{pulse} = 100 V, f_{rf} = 30 MHz, f_{pulse} = 500 kHz. (c) Pressure = 5 mTorr, power = 500 W, V_{pulse} = 100 V, f_{rf} = 30 MHz, f_{pulse} = 500 kHz. (d) Pressure = 5 mTorr, power = 300 W, V_{pulse} = 200 V, f_{rf} = 30 MHz, f_{pulse} = 500 kHz. (e) Pressure = 5 mTorr, power = 300 W, V_{pulse} = 100 V, f_{rf} = 13.56 MHz, f_{pulse} = 500 kHz kHz. (f) Pressure = 5 mTorr, power = 300 W, V_{pulse} = 100 V, f_{rf} = 30 MHz, f_{pulse} = 300 kHz.

Figure 10 exhibits the IADs bombarding the substrate corresponding to different external parameters. In figures 10(a) and (b), we can find that as the gas pressure increases, there would be more ions moving to the substrate with more dispersive angles, which is because larger pressure brings about more frequent collision progresses. Figures 10(a)
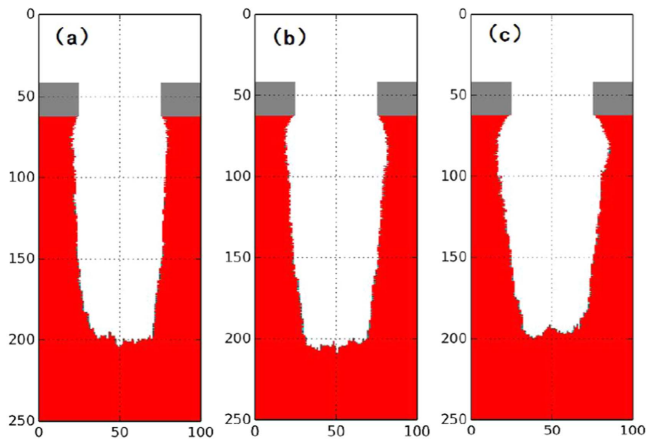
and (c) demonstrate that discharge power has obvious influences on the IADs, they become more concentrated when source power increases. From figures 10(a) and (d) we can reach the conclusion that as the amplitude of bias voltage is large, there would be more ions incident on the substrate with better directionality. The electrode potential drop only
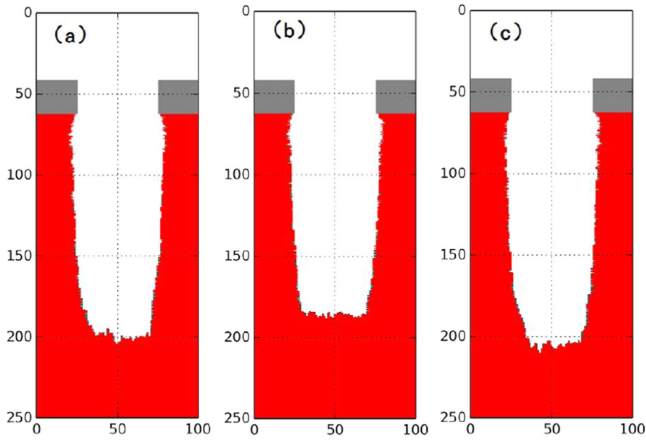
Figure 11. Feature profile evolution corresponding to the tailored bias voltage waveforms shown in figure 6, respectively. The discharge pressure is 5 mTorr, the source is 300 W, the RF-bias frequency is 30 MHz, the pulse-bias frequency is 500 kHz, and the bias voltage is 100 V.
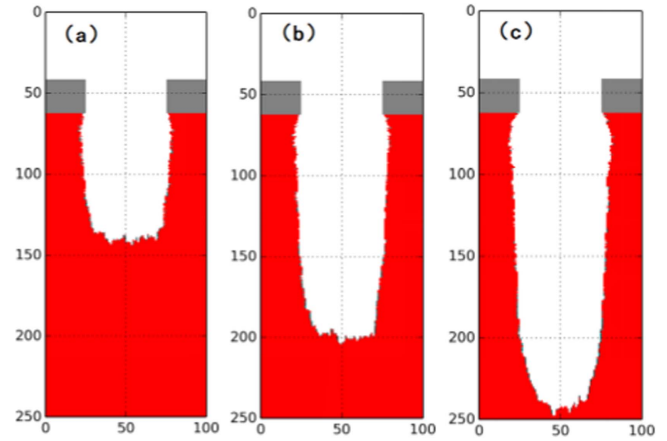
Figure 13. Feature profile corresponding to different source powers of (a) 100 W, (b) 300 W, (c) 500 W. The gas pressure is settled at 5 mTorr, the ratio of gas mixture is $Ar/Cl_2 = 80/20$, the RF-bias frequency is 30 MHz, the pulse-bias frequency is 500 kHz, and the amplitude of bias voltage is 100 V.

Figure 12. Feature profile corresponding to different discharge gas pressures of (a) 5 mTorr, (b) 10 mTorr, (c) 20 mTorr. The source power is settled at 300 W, the ratio of gas mixture is $Ar/Cl_2 = 80/20$, the RF-bias frequency is 30 MHz, the pulse-bias frequency is 500 kHz, and the amplitude of bias voltage is 100 V.

shows the pattern profile under different gas pressures. As the discharge pressure increases, there would be more low-energy ions generated, because the ion-neutral collisions will be more frequent, as shown in figures 9(a) and (b). In addition, the increasing pressure will result in more off-normal dispersive IADs, as shown in figures 10(a) and (b), which leads to more serious sidewall etching. The ion reflection occurring at the trench sidewall would cause micro-trenching in both sides of the trench bottom, and as the etching steps are carried out, the trench would be tapered.

Figure 13 shows the trench profile with different source power. Obviously, the etching depth rises rapidly as the RF power increases, which is because the fluxes of ions will be larger and the ion energies will be higher with source power increasing, as shown in figures 3–5, 9(a) and (c). The more energetic the ions, the larger the etch yield. The etching dependent on the aspect ratio results in the etch rate decreasing step-by-step and a sharper trench bottom with increasing etching depth.

Figure 14 exhibits the feature profile corresponding to different pulse-bias voltages. Apparently, the etching depth and rate will increase visibly as the amplitude of bias voltage increases, and we neglect the impact on the generation of plasma induced by the bias source, and so the fluxes of ions and neutrals remain invariable. The ions will obtain more energy as the potential drop increases when they are passing across the sheath with the bias voltage increasing, as shown in figures 9(a) and (d). The averaged higher ion-bombardment energy can contribute to the etch yield. Therefore, the etching trench would be etched more rapidly.

Figure 15 reveals the trench profile corresponding to different RF-bias frequency. We can find that the effect of RF-bias frequency increasing on the pattern profile is not monotonous. The corresponding IEDs are shown in figures 9(a) and (e). With the RF-bias frequency increasing, less ions could respond to the fast electric field oscillation instantaneously, then the width between low- and high-energy peaks decreases. The low-energy peak moving to a higher-energy area can lead

influences the vertical acceleration to the substrate irrespective of collisions between particles. Figures 10(a), (e) and (f) indicate that the influence of RF- and pulse-bias frequency on the IADs is not very obvious.

Figure 11 displays the trench profile evolution corresponding to the tailored bias voltage waveforms separately shown in figure 6. The pressure is 5 mTorr, source power is 300 W, and the ratio of gas mixture is $Ar/Cl_2 = 80/20$. The corresponding IEADs under different external conditions have been shown in figures 7 and 8. Intuitively, the trench profile with the bias voltage waveform shown in figure 6(b) applied on the electrode is more ideal as the IEDs corresponding to the waveform shown in figure 6(b) are more homogeneous than the IEDs corresponding to the waveforms shown in figures 6(a) and (c).
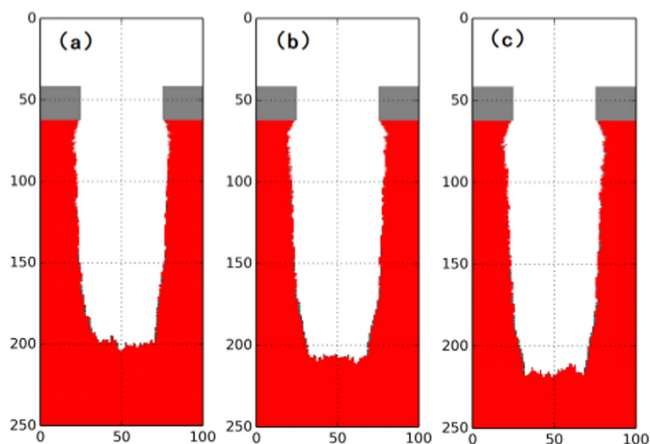
We study the feature profile evolution corresponding to different external parameters with applying the tailored bias waveform on the electrode, as shown in figure 6(a). Figure 12

Figure 14. Feature profile corresponding to different amplitude of bias voltages of (a) 100 V, (b) 150 V, (c) 200 V. The discharge pressure is settled at 5 mTorr, the source power is settled at 300 W, the ratio of gas mixture is $Ar/Cl_2 = 80/20$, the RF-bias frequency is 30 MHz, and the pulse-bias frequency is 500 kHz.
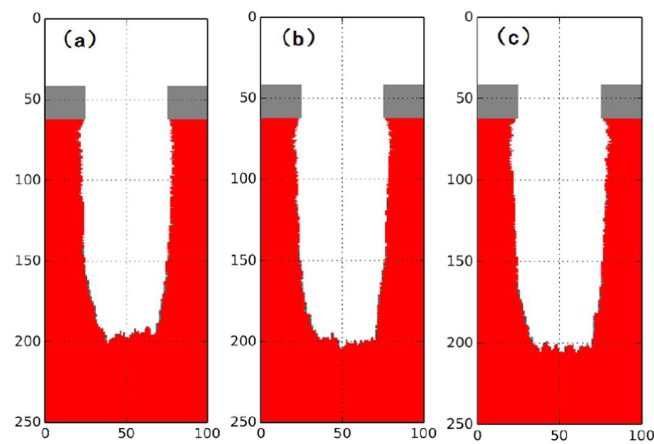
Figure 16. Feature profile corresponding to different pulse-bias frequency of (a) 300 kHz, (b) 500 kHz, (c) 800 kHz. The discharge gas pressure is settled at 5 mTorr, the source power is 300 W, the ratio of gas mixture is $Ar/Cl_2 = 80/20$, the RF-bias frequency is 30 MHz, and the amplitude of the bias voltage is 100 V.
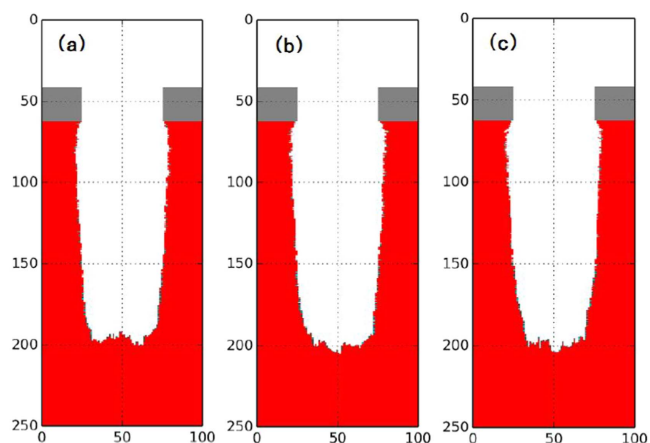
Figure 15. Feature profile corresponding to different RF-bias frequency of (a) 2 MHz, (b) 13.56 MHz, (c) 30 MHz. The discharge gas pressure is settled at 5 mTorr, the source power is 300 W, the ratio of gas mixture is $Ar/Cl_2 = 80/20$, the pulse-bias frequency is 500 kHz, and the amplitude of the bias voltage is 100 V.

to a higher etch rate, while the high-energy peak moving toward a smaller-energy area can result in the etch rate slowing down. The total etch rate would be affected by the two complex effects synergistically.

Figure 16 displays the feature profile corresponding to different pulse-bias frequency. Clearly, the depth increases slightly as the pulse-bias frequency increases, and the effects of pulse-bias frequency on the etching is very inconspicuous. The corresponding IEADs are shown in figures 9(a) and (f) and 10(a) and (f). With the pulse-bias frequency increasing, the position of the low-energy peak is almost immobile and the high-energy peak moves to the high-energy region slightly, and the influence of pulse-bias frequency on the IADs is not very obvious.

With the etch proceeding, the etching depth increases and more ions will reflect from the sidewall to the center of the trench bottom, which makes the trench scale more tapered. From another point of view, the etch process is a compromise

of deposition and etch. As the depth increases, less reactive ions can arrive at the etching bottom, which will lead the etching rate to slow down. At the same time, the deposition is chiefly related to the neutrals, which are not affected by the local electric field, and so the deposition progress becomes dominated before the end of the etching.

4. Conclusions

The rapid development of microelectronics manufacturing demands smaller feature sizes, which means more precise control of etching selectivity, anisotropy, and trench profile is needed. Flexible control of the IEADs is necessary to achieve atomic-scale resolution. Our paper studies the effects of different discharge parameters and tailored bias voltage waveform on the IEADs and trench profile evolution, which provides support for technical development and parameter optimization. A multi-scale model [12], including the reaction chamber model, sheath model, and trench model, has been provided to investigate the atomic layer etching of Si in inductively coupled argon/chlorine plasma with tailored bias voltage waveforms under different discharge parameters. Results indicate that these parameters influence the trench topography simultaneously. Higher discharge pressure results in more dispersive IADs, and then leads to more severe sidewall etching. In addition, the ion-reflection behavior can be influenced by the discharge pressure, which also affects the pattern profile evolution. The increasing of RF source power results in larger fluxes of ions, therefore inducing a higher etch rate. Less ions can respond to the fast oscillated electric field as the RF-bias frequency increases, so that the IEDs become more concentrated and the high-energy peaks move to low-energy areas. When the pulse-bias frequency increases, the low-energy areas are almost settled, and the high-energy peaks move toward the high-energy area slightly. Consequently, an appropriate bias frequency is very significant for the improvement of the etch rate. As the

amplitude of the bias voltage increases, the potential drop on the electrode will be larger, which means the ions will obtain more kinetic energy when passing through the sheath region.

As is known, the pulsed plasma can reduce the charging effects, and then improve the etching feature profile, and so we will use CFD-ACE+ to simulate the pulsed plasma discharge and investigate the influences of pulsed plasma on atomic layer etching with the tailored bias waveforms applied on the electrode synchronously in future work.

Acknowledgments

References

[1] Petit-Etienne C *et al* 2013 *J. Vac. Sci. Technol.* B **31** 011201
[2] Agarwal A and Kushner M J 2009 *J. Vac. Sci. Technol.* A **27** 37
[3] Shin H *et al* 2011 *Plasma Sources Sci. Technol.* **20** 055001
[4] Saussac J, Margot J and Chaker M 2009 *J. Vac. Sci. Technol.* A **27** 130
[5] Economou D J 2013 *J. Vac. Sci. Technol.* A **31** 050823
[6] Denpoh K 2014 *Jpn. J. Appl. Phys.* **53** 080304
[7] Wang M M and Kushner M J 2010 *J. Appl. Phys.* **107** 023309
[8] Liu Z *et al* 2015 *Plasma Sci. Technol.* **17** 560
[9] Hoekstra R J and Kushner M J 1996 *J. Appl. Phys.* **79** 2275
[10] Agarwal A *et al* 2009 *J. Appl. Phys.* **106** 103305
[11] Ranjan A *et al* 2016 *J. Vac. Sci. Technol.* A **34** 031304
[12] Zhang S Q *et al* 2014 *Vacuum* **99** 180
[13] Tinck S, Boullart W and Bogaerts A 2008 *J. Phys. D: Appl. Phys.* **41** 065207
[14] Sui J X *et al* 2016 *Plasma Sci. Technol.* **18** 666
[15] Dai Z L and Wang Y N 2004 *Phys. Rev.* E **69** 036403
[16] CFD-ACE+ 2009 *CFD-ACE+ Web Help* (Paris: ESI-Group)
[17] Ge J *et al* 2014 *Mod. Phys. Lett.* B **28** 1450149
[18] Lieberman M A and Lichtenberg A J 1994 *Principles of Plasma Discharges and Materials Processing* (New York: Wiley)
[19] Kim D and Economou D J 2002 *IEEE Trans. Plasma Sci.* **30** 2048
[20] Vitale S A, Chae H and Sawin H H 2001 *J. Vac. Sci. Technol.* A **19** 2197
[21] Hoekstra R J *et al* 1998 *J. Vac. Sci. Technol.* **16** 2102
[22] Hoekstra R J, Grapperhaus M J and Kushner M J 1997 *J. Vac. Sci. Technol.* A **15** 1913
[23] Cheng C C *et al* 1994 *J. Vac. Sci. Technol.* A **12** 2630